THE ASTRONOMICAL JOURNAL, 118:2158–2171, 1999 November

THE SHAPE AND FIGURE ROTATION OF THE DARK HALO OF NGC 2915

M. BUREAU,[1] K. C. FREEMAN, AND D. W. PFITZNER
Mount Stromlo and Siding Spring Observatories, Institute of Advanced Studies, Australian National University, Private Bag, Weston Creek Post Office, ACT 2611, Australia; bureau@strw.leidenuniv.nl

AND

G. R. MEURER
Department of Physics and Astronomy, Johns Hopkins University, 3700 North Charles Avenue, Baltimore, MD 21218
Received 1998 July 27; accepted 1999 June 10

ABSTRACT

NGC 2915 is a blue compact dwarf galaxy with a very extended H I disk. This disk shows a short central bar and extended spiral arms, both reaching far beyond the optical component. We use Tremaine & Weinberg's method to measure the pattern speed of the bar and spiral arms from H I radio synthesis data. Our measurements yield a pattern speed $\Omega_p = 0.21 \pm 0.06$ km s^{-1} arcsec^{-1} (8.0 ± 2.4 km s^{-1} kpc^{-1} for $D = 5.3$ kpc), in disagreement with the general view that corotation in barred disks lies just outside the end of the bar, but consistent with recent models of barred galaxies with dense dark matter halos. Our adopted bar semilength, $r_b \approx 180''$, puts corotation at more than $1.7r_b$. The existence of the pattern is also problematic. Because NGC 2915 is isolated, gravitational interactions cannot account for the structure observed in the H I disk. We also demonstrate that the low surface density observed in the disk and the location of the pseudorings make it unlikely that swing amplification or bar-driven spiral arms could explain the bar and spiral pattern. Based on the similarity of the dark matter and H I surface density profiles, we discuss the possibility of dark matter distributed in a disk and following closely the H I distribution. This disk then becomes gravitationally unstable and can naturally form a bar and spiral pattern. However, this explanation is difficult to reconcile with some properties of NGC 2915. We also consider the effect of a massive and extended triaxial dark matter halo with a rotating figure. The existence of such halos is supported by cold dark matter simulations showing strongly triaxial dark halos with slow figure rotation. The observed structure of the H I disk can then arise through forcing by the rotating triaxial figure. We associate the measured pattern speed in NGC 2915 with the figure rotation of its dark halo.

Key words: dark matter — galaxies: evolution — galaxies: formation — galaxies: individual (NGC 2915) — galaxies: kinematics and dynamics — galaxies: structure

1. INTRODUCTION

About 30% of spiral galaxies are strongly barred. This fraction is roughly doubled if weaker barlike asymmetries are included, and it reaches almost unity if K-band images and quantitative methods are used for classification (see, e.g., Seiger & James 1998). Studying barred spiral galaxies is therefore an important part of galactic structure and dynamics, and we refer the reader to the review by Sellwood & Wilkinson (1993).

The form of the potential and the bar pattern speed (Ω_p) are the most important quantities determining the structure and dynamics of a barred disk. N-body simulations of bars (e.g., Sellwood 1981; Combes & Sanders 1981) and analytical calculations (e.g., Contopoulos 1980; Contopoulos & Grosbøl 1989) have shown that for bars to be self-consistent, their pattern speed should be such that corotation occurs outside the end of the bar. However, measuring the pattern speed of bars is not an easy task, and most methods are rather indirect (see Schwarz 1981, 1984; Athanassoula 1992b; Canzian 1993). The method proposed by Tremaine & Weinberg (1984) is the only direct method, being based on observables alone. However, because of the assumptions it makes, the method is rarely applicable to real galaxies, and it has been applied successfully to only two objects so far (NGC 936, Kent 1987; Merrifield & Kuijken 1995; NGC 4596, Gerssen, Kuijken, & Merrifield 1999). In this paper, we apply the Tremaine & Weinberg (T-W) method to the galaxy NGC 2915, a blue compact dwarf (BCD) galaxy with a very extended H I disk (see Meurer, Mackie, & Carignan 1994, hereafter MMC94; Meurer et al. 1996, hereafter MCBF96). This disk shows a late barred spiral galaxy morphology extending far beyond the optical component.

While the formation of bars is now fairly well understood, the formation of the spiral patterns seen in many galaxic disks remains an open issue. Various mechanisms have been proposed. We consider the most prominent ones in this paper: gravitational interactions (e.g., Noguchi 1987), swing amplification of spiral density waves (e.g., Toomre 1981), and bar-driven spiral arms (e.g., Byrd et al. 1994). We show that none of these is likely to explain the bar and spiral arm structure observed in the H I disk of NGC 2915.

This problem leads us to consider the background mass distribution in NGC 2915. To explain their flat rotation curves, disks are commonly believed to be immersed in massive dark halos (e.g., Carignan & Freeman 1985). Although the shape of such halos is usually assumed to be spherical, there is little observational information on this subject, and other shapes are clearly possible (see Trimble 1987 and Carr 1994 for reviews). For NGC 2915, we demonstrate that a simple rigid spherical halo is unable to

[1] Current address: Sterrewacht Leiden, Postbus 9513, NL-2300 RA Leiden, Netherlands.

explain the properties of the H I disk. We therefore consider other dark matter distributions, including (1) dark matter distributed in a thin disk following the H I surface density distribution and (2) dark matter distributed in an extended triaxial halo with a slowly rotating figure.

In § 2, we discuss the T-W method to measure the pattern speed of bars and review its past applications. In § 3, we describe the properties of NGC 2915 and measure its pattern speed. The issues of self-consistency and multiple pattern speeds are touched upon in § 4, and in § 5 we discuss the possible formation mechanisms for the bar and spiral pattern. In § 6, we consider two particular models for the dark matter distribution of NGC 2915.

2. PATTERN SPEED MEASUREMENT

2.1. *Indirect Methods*

Many indirect methods have been devised to measure the bar pattern speed Ω_p in barred spiral galaxies, and we discuss two of them here. The first relies on the theory of resonance ring formation (Schwarz 1981, 1984; see also Byrd, Ousley, & Dalla Piazza 1998). It is possible to identify morphological features in the disk of a barred galaxy, such as rings, with the locations of known resonances. Using the circular velocity curve and derived epicyclic frequency, the bar pattern speed can then be inferred (see Ryder et al. 1996 for recent applications to NGC 1433 and NGC 6300). We apply this method to NGC 2915 in § 5. Second, it is possible to construct hydrodynamic models of the gas flow in a galaxy (often to reproduce H I observations, because of their full kinematic coverage). Hydrodynamic models depend on several parameters of the potential, including Ω_p, so the best-fitting model gives an estimate of the bar pattern speed (see Lindblad & Kristen 1996 and Lindblad, Lindblad, & Athanassoula 1996 for recent applications to NGC 1300 and NGC 1365). Sellwood & Wilkinson (1993) review many such barred-galaxy studies.

Although these indirect methods yield useful information about pattern speeds, it is clearly preferable to have a direct measurement, with no dependence on theoretical arguments or comparison with dynamical models. We will thus pursue these indirect methods only to check the consistency of more direct measurements.

2.2. *Direct Methods*

Tremaine & Weinberg (1984) showed that the pattern speed of a barred disk galaxy can be derived from the observed kinematics of a tracer population if (1) a unique, well-defined disk pattern speed Ω_p exists and (2) the luminosity density of the tracer satisfies the continuity equation. With these conditions, the pattern speed is given by

$$\Omega_p \sin i = \frac{\int_{-\infty}^{\infty} h(y)dy \int_{-\infty}^{\infty} \Sigma(x, y)[\bar{v}_{\rm los}(x, y) - v_{\rm sys}]dx}{\int_{-\infty}^{\infty} h(y)dy \int_{-\infty}^{\infty} \Sigma(x, y)x\,dx}, \quad (1)$$

where i is the disk inclination, Σ is the surface brightness distribution of the tracer, $\bar{v}_{\rm los}$ is the mean line-of-sight velocity of the tracer, $v_{\rm sys}$ is the systemic velocity of the galaxy, and (x, y) are Cartesian coordinates on the plane of the sky, with the origin at the center of the galaxy and the x-axis parallel to the line of nodes (i.e., the apparent major axis for an intrinsically round disk). These quantities are all observable. The function $h(y)$ is an arbitrary weighting function (see Tremaine & Weinberg 1984). Although the method was developed to measure bar pattern speeds, it can be applied equally to any strong and fairly open pattern, such as spiral arms.

The continuity assumption is valid for dust-free old stellar populations but may well break down in dusty systems, or when using gas as a tracer (because of the possibility of ionization, molecular conversion, optical thickness, etc.). In fact, although Tremaine & Weinberg (1984) succeeded in applying their method to an artificial data set generated from an N-body simulation, they failed when applying it to H I data from the barred spiral galaxy NGC 5383 (Sancisi, Allen, & Sullivan 1979). The method is sensitive to noise because only the nonsymmetric (i.e., odd in x) part of Σ contributes to the integrals in equation (1).

Kent (1987) applied the T-W method to the barred spiral galaxy NGC 936. The stellar component of NGC 936 is ideal for this application because it has a strong bar, high surface brightness, and high rotation velocity and is devoid of dust and star formation. The orientation of the system is also favorable. Kent carefully estimated the sources of error in measuring Ω_p. Unfortunately, the relatively poor quality of the kinematic data (by today's standards) led to inconclusive results. He derived an average pattern speed $\Omega_p = 8.4 \pm 2.9$ km s^{-1} arcsec^{-1} ($\Omega_p = 104 \pm 36$ km s^{-1} kpc^{-1} for $D = 16.6$ Mpc). With Kormendy's (1984) rotation curve, corrected for noncircular motions, and a deprojected bar length of 52″, corotation lies between 0.54 and 1.21 bar semilengths. This is only marginally consistent with the general result from orbital calculations and self-consistent models of barred spirals that corotation must occur outside the end of the bar and is generally located just beyond its ends (see, e.g., Sellwood 1981; Teuben & Sanders 1985; Athanassoula 1992b).

Merrifield & Kuijken (1995; see also Kuijken & Merrifield 1996) reapplied the T-W method to NGC 936, this time with better data and methods. They did not use equation (1) directly but rather used the equivalent formula

$$\Omega_p \sin i = (\langle \bar{v}_{\rm los} \rangle - v_{\rm sys})/\langle x \rangle \quad \text{(for a given } y), \quad (2)$$

where the angle brackets represent luminosity-weighted averages along the slit. The advantage of this procedure is that the long-slit data can be co-added along the spatial axis to measure $\langle \bar{v}_{\rm los} \rangle$, and along the dispersion axis to measure $\langle x \rangle$, yielding higher signal-to-noise measurements. To obtain an unbiased measure of $\langle \bar{v}_{\rm los} \rangle$, Merrifield & Kuijken (1995) also used a deconvolution algorithm allowing for asymmetric Doppler broadening of the spectral lines. They obtained a well-defined average pattern speed $\Omega_p = 4.8 \pm 1.1$ km s^{-1} arcsec^{-1} ($\Omega_p = 60 \pm 14$ km s^{-1} kpc^{-1} for $D = 16.6$ Mpc). This value puts corotation at $69'' \pm 15''$, or 1.3 ± 0.3 bar radii, in good agreement with theoretical expectations.

Using the same procedure, Gerssen et al. (1999) recently measured the bar pattern speed in the SBa galaxy NGC 4596, which is similar to NGC 936. They derive a pattern speed $\Omega_p = 3.9 \pm 1.0$ km s^{-1} arcsec^{-1} ($\Omega_p = 52 \pm 13$ km s^{-1} kpc^{-1} for $D = 15.7$ Mpc). This again indicates a fast bar, placing corotation just outside the end of the bar, at approximately 1.25 bar semilengths (see also Kent 1990).

3. NGC 2915

3.1. *Background*

NGC 2915 is a nearby isolated BCD galaxy. MMC94 carried out optical imaging and spectroscopy of NGC 2915

to study its structure, stellar populations, and star formation history. MCBF96 obtained radio synthesis data to study the H I distribution and kinematics of NGC 2915, as well as to constrain its overall mass distribution (including dark matter). Table 1 summarizes the basic properties of NGC 2915.

The photometry of MMC94 shows that NGC 2915 has two distinct stellar populations: (1) an exponential red diffuse population in the outer parts ($r \geq 35'' = 0.90$ kpc), with a scale length $\alpha_B^{-1} = 25''.6$ (660 pc), an extrapolated central surface brightness $B_c = 22.44$ mag arcsec^{-2} (corrected for inclination and extinction), and constant color, and (2) a slightly peaked core population ($r < 35''$), with increasingly bluer color toward the center. The diffuse population is similar to that of dwarf elliptical galaxies, but the core is lumpy, contains a young stellar population, and is the locus of high-mass star formation. Spectroscopy in the core shows strong Balmer and Ca II H + K absorption lines, and strong narrow emission lines with ratios typical of high-excitation, low-metallicity H II regions. A velocity difference of 60 km s^{-1} is detected across the inner galaxy. If this gradient is due solely to rotation, it corresponds to a deprojected rotational velocity of $V_r = 50 \pm 21$ km s^{-1} at $r = 32''$ (neglecting the effects of the bubbles seen in Hα by Marlowe et al. 1995). The associated mass for the optical core, $M_{\rm core} = 4.8 \times 10^8\ M_\odot$, with a mass-to-light ratio $M_{\rm core}/L_B = 1.3(M/L_B)_\odot$.

The neutral hydrogen observations of NGC 2915 (MCBF96) reveal an H I distribution very different from the optical. Figure 1 shows the naturally weighted total H I intensity map overlaid on an optical image of NGC 2915. The H I distribution is unusually extended, up to $5D_{{\rm Ho},B}$ ($22.6\alpha_B^{-1}$), and it has a striking late-type barred spiral galaxy morphology, with two extended spiral arms starting at the end of a central bar. This is unusual because bars are generally H I–poor. At higher resolution, the H I bar is resolved into two clouds; its semilength is about 2'.4 (3.7 kpc) and it corresponds roughly in position, orientation, and size to the optical emission. The H I surface density profile is tabulated in Table 2. The total H I mass $M_{\rm H\,I} = 9.6 \times 10^8\ M_\odot$, while the H I mass in the bar is only about (5–7.5) $\times 10^7\ M_\odot$. Figure 2 shows the naturally weighted H I velocity field of

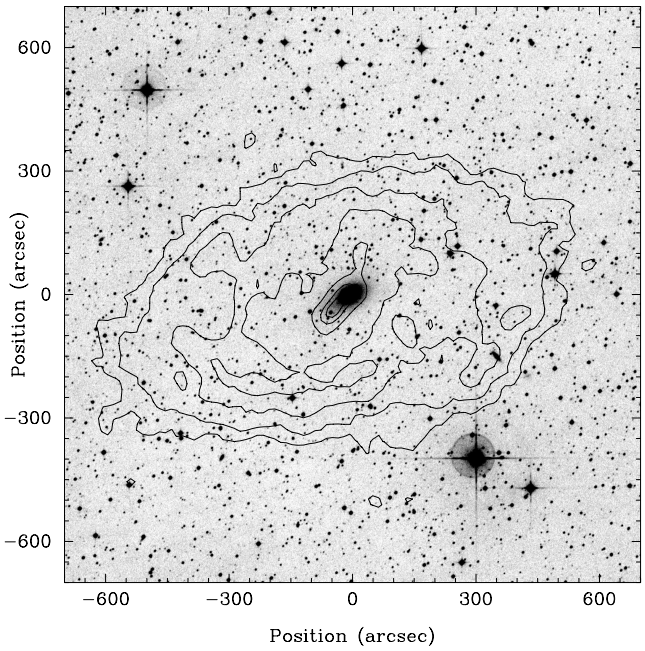

FIG. 1.—Naturally weighted total H I intensity map (MCBF96), overlaid on an optical image of NGC 2915 (Digitized Sky Survey). The beam is 45″ × 45″. Contour levels are 2.5%, 7.5%, 15%, 25%, 50%, 75%, and 90% of the peak H I surface brightness of 3.1 Jy beam^{-1} km s^{-1} ($N_{\rm HI} = 1.71 \times 10^{21}$ cm^{-2}).

NGC 2915 (MCBF96), again overlaid on an optical image. It clearly shows the pattern of a rotating disk (with an oval distortion) and suggests the presence of a warp in the outer parts. MCBF96 derived a rotation curve for NGC 2915 using the standard tilted-ring algorithm ROTCUR (Begeman 1989). The position angle varies by about 15° and the inclination by about 10° outside the barred region (where the effects of the bar and a possible warp are hard to disentangle), supporting the suggestion that a warp is present in the outer disk. The H I velocity dispersion outside the bar region is the usual $\sigma_v \approx 8$ km s^{-1}, but it increases up to 40 km s^{-1} in the central regions (see Table 2), a value comparable to the rotation velocities obtained from

TABLE 1

BASIC PROPERTIES OF NGC 2915

Quantity	Value	Reference
Position (J2000.0)	$\alpha = 9^{\rm h}26^{\rm m}11^{\rm s}.83$	1
	$\delta = -76°37'35''.8$	1
Heliocentric velocity	$V_\odot = 468 \pm 5$ km s^{-1}	2, 3
Distance	$D = 5.3 \pm 1.6$ Mpc	1
Classification	I0/BCD	1
Total apparent B magnitude	$m_{B_T} = 13.34$ mag	1
Total absolute B magnitude	$M_{B_T} = -15.90$ mag	1
B disk scale length	$\alpha_B^{-1} = 25''.6$ (660 pc)	1
Corrected B central surface brightness	$B_c = 22.44$ mag arcsec^{-2}	1
B Holmberg radius ($\mu_{B,0} = 26.6$ mag arcsec^{-2})	$R_{{\rm Ho},B} = 1'.9$ (2.93 kpc)	1
Total H I flux	$F_{\rm HI} = 145$ Jy km s^{-1}	2
Total H I mass	$M_{\rm HI} = 9.58 \times 10^8\ M_\odot$	2
H I velocity width	$W_{20} = 170$ km s^{-1}	2
H I extent ($N_{\rm H\,I,0} = 5 \times 10^{19}$ cm^{-2})	$R_{\rm HI} = 9'.7$ (14.9 kpc)	2
Dust mass	$M_{\rm dust} = 1.05 \times 10^4\ M_\odot$	3
Total mass (within $r \approx 600'' = 15.4$ kpc)	$M_{\rm tot} = 2.7 \times 10^{10}\ M_\odot$	2

REFERENCES.—(1) MMC94; (2) MCBF96; (3) Schmidt & Boller 1992.

TABLE 2

STRUCTURAL AND KINEMATIC PROFILES OF NGC 2915

r (arcsec)	μ_{HI} $M_\odot$ pc^{-2}	μ_B B mag arcsec^{-2}	V_c km s^{-1}	σ_v km s^{-1}	Ω km s^{-1} arcsec^{-1}	κ km s^{-1} arcsec^{-1}
27.5	8.90	22.55	39.0	33.4	1.42	2.37
52.5	6.35	23.97	53.0	28.8	1.01	1.76
77.5	4.10	25.11	65.0	23.0	0.84	1.44
102.5.....	3.17	26.26	72.7	20.8	0.71	1.15
127.5.....	2.53	27.20[a]	76.0	15.6	0.60	0.93
152.5.....	2.26	28.26[a]	79.2	11.9	0.52	0.81
177.5.....	2.32	29.32[a]	81.4	10.7	0.46	0.69
202.5.....	2.36	30.38[a]	82.5	9.9	0.41	0.60
227.5.....	2.12	31.44[a]	82.8	9.2	0.36	0.48
252.5.....	1.75	32.50[a]	80.4	10.1	0.32	0.41
277.5.....	1.49	33.56[a]	80.4	10.1	0.29	0.42
302.5.....	1.41	34.62[a]	80.9	9.3	0.27	0.38
327.5.....	1.46	35.68[a]	80.7	8.7	0.25	0.35
352.5.....	1.43	36.74[a]	80.8	8.3	0.23	0.34
377.5.....	1.23	37.80[a]	82.0	8.8	0.22	0.32
412.5.....	1.09	39.28[a]	82.3	8.6	0.20	0.30
457.5.....	0.89	41.19[a]	83.8	8.1	0.18	0.28
502.5.....	0.67	43.10[a]	85.5	8.1	0.17	0.28
547.5.....	0.48	45.01[a]	88.5	8.1	0.16	0.29
592.5.....	0.32	46.92[a]	93.9	7.7	0.16	0.30

[a] Extrapolated value from the exponential fit to the outer parts of the disk of MMC94.

ROTCUR. This indicates that pressure support is important in the center of NGC 2915. MCBF96 applied an asymmetric drift correction to the rotation curve to produce the circular velocity curve needed for mass modeling. The circular velocity is tabulated in Table 2. It increases rapidly with radius in the inner parts, reaching 80 km s^{-1} by $r = 150''$ (3.9 kpc), stays flat until $r = 400''$–$450''$ (10.3–11.6 kpc), and increases again up to $\approx$90 km s^{-1} at the last measured point ($r \approx 600'' = 15.4$ kpc).

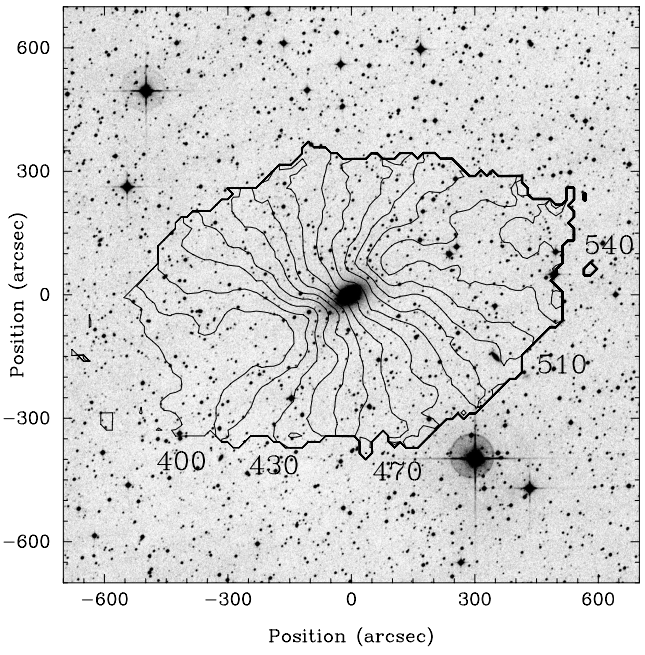

FIG. 2.—Naturally weighted H I velocity field (MCBF96), overlaid on an optical image of NGC 2915 (Digitized Sky Survey). The beam is $45'' \times 45''$ and the velocity resolution is 6.62 km s^{-1}. Contours are heliocentric velocities separated by 10 km s^{-1}. A few contours are identified.

MCBF96 constructed three-component mass models to interpret the circular velocity curve. The models were composed of (1) a stellar disk, obtained from the surface brightness profiles of MMC94 (the mass-to-light ratio M/L_B is a free parameter), (2) an H I disk, based on their observations, and (3) a spherical dark halo (two density distributions were used, both with a central density ρ_0 and core radius r_c as free parameters). All models are dominated by dark matter at all radii. In fact, NGC 2915 is one of the darkest disk galaxies known. Its dark matter core is very dense and compact, which may prove crucial to understanding its pattern speed (see § 4.1). MCBF96's best-fit model[2] has $M/L_B = 1.2\,(M/L_B)_\odot$, $\rho_0 = 0.10 \pm 0.02\ M_\odot$ pc^{-3}, and $r_c = 1.23 \pm 0.15$ kpc, yielding a total mass $M_T = 2.7 \times 10^{10}\ M_\odot$, $M_T/L_B = 76\ (M/L_B)_\odot$, and $M_{\rm dark}/M_{\rm lum} = 19$ within the last measured point.

3.2. *Pattern Speed*

We now attempt to measure the pattern speed Ω_p of the figure in the disk of NGC 2915 using the H I data of MCBF96. As mentioned in § 2.2, the continuity equation imposes a strong constraint on the applicability of the T-W method, and gaseous systems are usually thought to be poor candidates for a measurement. NGC 2915 is an unusual galaxy, however, and we argue that the T-W method should work for its H I distribution. First, because the stellar component of NGC 2915 is confined to the inner regions of its H I distribution and the star-forming core to the very center of the H I bar, there is no source of ionizing photons over most of the H I disk (except for the weak metagalactic radiation field and possibly some radiation from the distant core reaching the warped regions). Meurer et al. (1999) searched for H II regions in the outer disk but

[2] Their model D, with a dark matter density distribution $\rho(r) = \rho_0[1 + (r/r_c)^2]^{-1}$.

found none. This situation is in contrast to that in NGC 5383, where Tremaine & Weinberg (1984) failed to obtain a reliable measurement of the pattern speed using neutral hydrogen observations. Second, the H I column density is low enough in most of the disk (where the velocity dispersion $\sigma_v \approx 8$ km s^{-1}) that optical thickness should not affect the observed H I intensity. Only in the inner parts of the bar, where the optical disk lies, does the column density reach $N_{\rm HI} = 10^{21}$ cm^{-2}, but there the H I velocity dispersion is larger ($\sigma_v \approx$ 20–40 km s^{-1}) so again the optical thickness is expected to be low. No molecular data on NGC 2915 are available in the literature, so we do not have any information on possible H I–molecule conversion at this point. However, the low H I column density again suggests that this effect is not important. Nevertheless, to properly constrain its molecular content, we are currently pursuing molecular line observations of NGC 2915. For all these reasons, and because the bar and spiral arm pattern is clear and strong, we believe that the T-W method applied to the H I synthesis data of NGC 2915 should give a realistic measure of its pattern speed. We note that the orientation of the system is ideal, with the disk at intermediate inclination and the bar about 30° from the major axis of the disk.

We apply the T-W method to NGC 2915 using MCBF96's naturally weighted total H I intensity map and velocity field (see Figs. 1 and 2). The additional structural and kinematic parameters required to use the T-W method (see § 2.2) are all provided by the tilted-ring analysis of MCBF96. We use averages of their parameters for the outer disk, outside of the barred region ($r > 150''$): the center of the disk $(x_c, y_c) = (0'', 0'')$ with respect to the pointing center [$\alpha = 9^{\rm h}26^{\rm m}11^{\rm s}$, $\delta = -76°37'35''$, (J2000)], $v_{\rm sys} = 467$ km s^{-1}, and the position angle of the line of nodes P.A. = 117°. We use equation (1) directly, without a weighting function $h(y)$, and for all possible positions y (equivalent to using $h(y) = \delta(y - y_0)$ for all y_0). Because the major axis traces the position of the line of nodes, y is effectively the position of the integration axis along the minor axis of the galaxy. Each offset y provides an independent measurement of the pattern speed. The coordinate system is shown in Figure 3, and Figure 4*a* shows the derived pattern speed as a function of the offset y. The measurements are roughly consistent with each other for most offsets. Only for a few isolated points and for offsets between 0″ and 200″ toward the northeast side of the galaxy (positive offsets) are the values of $\Omega_p \sin i$ significantly discrepant (but see below). We recall that the T-W method assumes a unique pattern speed for the whole disk, so all offsets should yield similar pattern speeds.

The discrepant region is associated with the northernmost of the two clouds identified by MCBF96, located at the northern end of the bar. Around that region, both the total H I intensity distribution and the velocity field show a strong deviation from their large-scale pattern. The discrepancies in the derived pattern speeds probably arise from the fact that the cloud breaks the pattern in the density distribution and/or the velocity field, an effect to which equation (1) is very sensitive. Away from this problematic region, the pattern speed is well defined: the entire southwest half of the galaxy and the farthest regions in the northeast half all yield fairly consistent values for $\Omega_p \sin i$. We thus believe that the T-W method works using the H I component of NGC 2915 and yields a reliable estimate of its pattern speed.

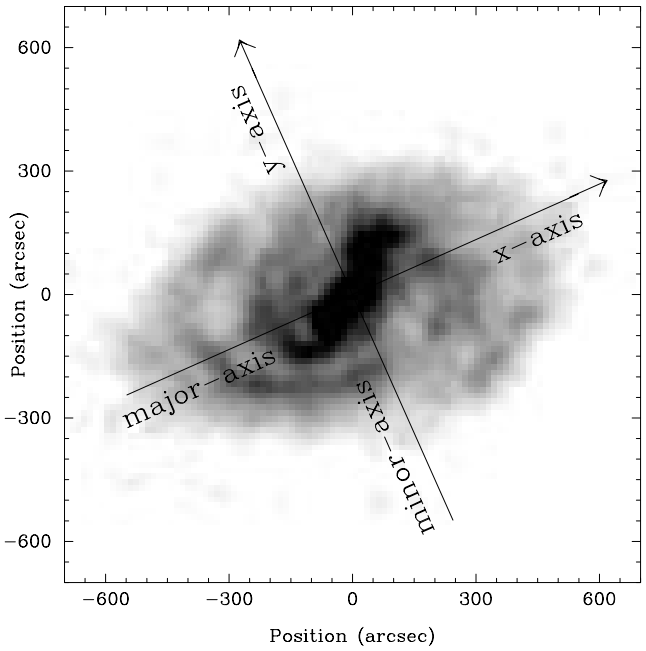

FIG. 3.—Schematic for the Tremaine-Weinberg method calculations (eq. [1]), overlaid on a gray-scale image of the naturally weighted total H I intensity map (45″ × 45″ beam) (MCBF96).

In our calculations, we assumed that the parameters required to use the T-W method were fixed over the whole disk. The center of the disk is well defined, and only the x-component of the center (x_c) affects the calculations anyway. The systemic velocity is also well constrained, with a small uncertainty of a few kilometers per second. However, as shown by the tilted-ring analysis of MCBF96, both the inclination i and in the NGC 2915 position angle P.A. vary significantly with radius. A change in inclination affects the pattern speed measurements only through the deprojection, but a change in position angle materially affects the calculations. We have therefore reapplied the T-W method to the H I data using a range of values for x_c, $v_{\rm sys}$, and P.A. Although no combination of parameters yields perfectly equal pattern speeds for all offsets, most cases with plausible values show a regular behavior, with only a restricted range of offsets having very discrepant measurements.

A typical good case is presented in Figure 4*b*. For all combinations of parameters, the flat portions of the $\Omega_p \sin i$ "distribution" always lie between $\Omega_p \sin i = 0.12$ km s^{-1} arcsec^{-1} and $\Omega_p \sin i = 0.22$ km s^{-1} arcsec^{-1}. We therefore adopt $\Omega_p \sin i = 0.17 \pm 0.05$ km s^{-1} arcsec^{-1} ($\Omega_p \sin i = 6.6 \pm 1.9$ km s^{-1} kpc^{-1} for $D = 5.3$ Mpc) as our estimate of the pattern speed in NGC 2915. The uncertainty given represents half the range of measured values for $\Omega_p \sin i$ and is not a standard error estimate. It is clear from our measurements that the formal errors are much smaller than the errors introduced by the uncertainties in the structural and kinematic parameters of the disk or the errors introduced because we are working with a less than perfect system. From the outer parts of the disk again, we get an average inclination $i = 56° \pm 3°$. This yields a deprojected pattern speed $\Omega_p = 0.21 \pm 0.06$ km s^{-1} arcsec^{-1} (8.0 ± 2.4 km s^{-1} kpc^{-1}).

The 30% uncertainty in Ω_p is comparable to that achieved by Merrifield & Kuijken (1995) for NGC 936, but

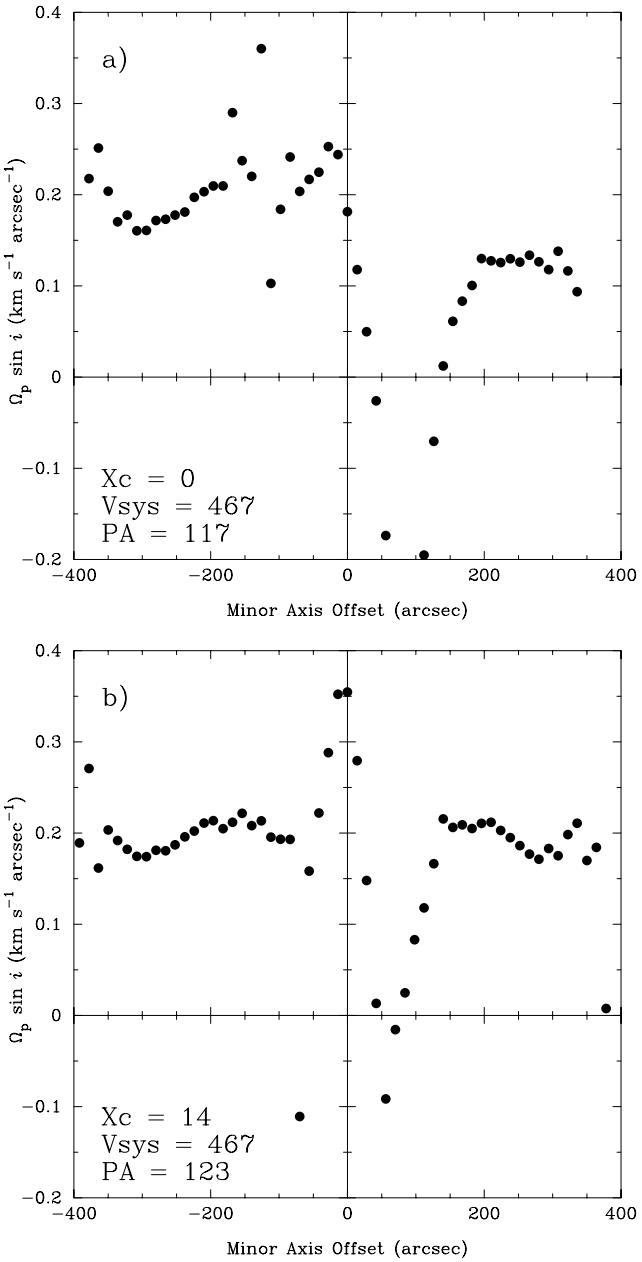

FIG. 4.—Tremaine-Weinberg method measurements of the pattern speed in NGC 2915. (*a*) The case with tilted-ring model best-fit parameters (MCBF96). (*b*) Typical good case. Parameters are indicated in the bottom left corner of each panel.

is still large given that we are using gas kinematics with the advantage of complete two-dimensional spatial coverage. On the other hand, our error estimate (half the range of measured values) is very conservative. As suggested by Tremaine & Weinberg (1984), we tried using odd weighting functions [e.g., $h(y) = \delta(y - y_0) - \delta(y + y_0)$; y_c now affects the calculations directly]. Such weighting eliminates the contribution of perturbations with odd azimuthal wavenumbers to the integrals in equation (1) and diminishes the effect of centering errors. However, it did not improve our results, mainly because discrepant regions on one side of the minor axis contaminate the combined measurements from both sides. Although we cannot exclude the possibility that the continuity equation is not fully satisfied for H I in some parts of NGC 2915 (particularly the central regions), the main sources of uncertainty in our measurements are the poorly constrained disk parameters (mainly the position angle), in turn related to the presence of a strong warp in the outer disk. Tremaine & Weinberg (1984) note that a warp may affect the pattern speed determination, acting as a non-axisymmetric perturbation with zero pattern speed. There may be some short-lived features in the disk (such as the structure seen near the northernmost cloud), but their effect is hard to quantify. We repeated the calculations using only the inner barred region of the galaxy, but the results were inconclusive. It is far from clear that the method should work in such a case anyway, as the integrals in equation (1) should extend over the whole system.

4. NATURE OF THE PATTERN

4.1. *Self-consistent Bars*

Orbital calculations in barred-disk potentials show that bars should end at or inside their corotation radii (see, e.g., Contopoulos 1980; Athanassoula 1992a; for a review, see Contopoulos & Grosbøl 1989). The argument is that the bar-shaped x_1 orbits, believed to support self-consistent bars, extend close to but not past corotation [where $\Omega_p = \Omega(r)$].

N-body studies show that rotationally supported stellar disks are globally unstable to bisymmetric distortions and quickly form strong bars. This is seen in both two-dimensional (e.g., Sellwood 1981; Athanassoula & Sellwood 1986) and three-dimensional (e.g., Combes & Sanders 1981; Raha et al. 1991) simulations. These instabilities can be identified with the dominant linear modes found in analytical global stability analyses of axisymmetric disks (Kalnajs 1971, 1977). The main characteristic of the stellar bars formed in such simulations is that they are fast, generally ending at or just inside corotation.

This property of self-consistent barred disks does not appear to hold in NGC 2915; the gaseous bar ends well within corotation. We take the ends of the bar to be where the density of the rectangularly shaped central component of the H I distribution drops rapidly. This is also the region where the spiral arms start. The observed semilength of the bar is then about 145″, with a deprojected value $r_b \approx 180''$. Our adopted pattern speed $\Omega_p = 0.21 \pm 0.06$ km s^{-1} arcsec^{-1} (see § 3.2) and MCBF96's circular velocity curve (Table 2) put corotation at a radius $r_{co} = 390^{+\infty}_{-80}$ arcsec (see Fig. 7). The ratio of corotation to the bar semilength is thus very large, $r_{co}/r_b > 1.7$, indicating a *slowly* rotating bar.

Such a slow pattern speed is inconsistent with the simulations mentioned above. However, all these studies used models in which luminous mass dominates the inner (optical) regions of the galaxies. MCBF96 showed that this is not the case in NGC 2915, where dark matter dominates at all radii. In fact, the dense and compact dark matter core of NGC 2915 may be the clue to its slow pattern speed. Dense dark halos have been predicted to slow down bars significantly, because the bar can transfer angular momentum to the outer disk and halo efficiently through dynamical friction (see Sellwood 1980; Weinberg 1985; Debattista & Sellwood 1998). Because dark matter is generally more important in low-luminosity spirals, in which it is difficult to measure pattern speeds, present support for these models is marginal (see, e.g., Elmegreen 1996). NGC 2915 may thus represent the strongest observational evidence so far for bar deceleration by dark halos with high central densities. The

mass model of MCBF96, the N-body simulations of Debattista & Sellwood (1998), and the bar pattern speed measured here are all consistent with each other. However, the effects of gaseous processes on bar deceleration remain to be fully investigated. These have not been taken into account in the aforementioned studies, but they are certainly relevant in the case of NGC 2915. Gas inflow, in particular, could speed up the bar.

4.2. *Bar or Spiral Arm Pattern Speed?*

The T-W method measures the pattern speed of a disk, assumed to be unique. While it was designed to measure bar pattern speeds, it applies equally to any pattern present in a disk, as long as it is strong enough. It is therefore important to establish which component's pattern speed we are measuring. Are we measuring the pattern speed of the bar, the spiral arms, or a common pattern speed for both?

Sellwood & Sparke (1988) suggest that spiral arms in barred spiral galaxies could have a different (lower) pattern speed than the bar. Their work was aimed primarily at explaining the presence of dust lanes on the inner edge of spiral arms in many objects. A lower pattern speed for the spiral pattern would allow the gas to overtake that pattern and therefore lie within its corotation radius in that region, while still retaining the view that bars end just inside *their* corotation radii. Sellwood & Sparke's (1988) suggestion is supported by N-body simulations of barred galaxies showing outer spiral patterns slower than the bars (Sparke & Sellwood 1987).

Tagger et al. (1987) and Sygnet et al. (1988) develop the idea that the nonlinear coupling of two modes with different pattern speeds could sustain spiral structures for a long time. For the mechanism to be efficient, resonances of the two patterns must be closely spaced. They observe this effect in many N-body simulations, where the corotation radius of the bar and the inner Lindblad resonance (ILR) of the spiral pattern are very close (this is also the region where the bar ends and the spiral arms begin). The beat wave generated is then axisymmetric and close to its Lindblad resonance, and it couples nonlinearly to the bar and spiral arms.

If we assume that the pattern speed measured here is that of the spiral arms and that the corotation radius of the bar lies close to the ILR of the spiral pattern, as suggested by Tagger et al. (1987) and Sygnet et al. (1988), we obtain a bar corotation radius $r_{co} < 50''$ (see Fig. 7), well inside the bar observed in H I ($r_b \approx 180''$). Such a view would be difficult to defend, considering the body of analytical and numerical work that requires the corotation radius of the bar to lie at or beyond its end. This is a strong indication that we are in fact measuring the pattern speed of the bar, but the argument is weakened by the small self-gravity of the disk (see § 5.2), which hinders the proposed mechanism.

Considering the form of equation (1), we see that for small minor-axis offsets ($y < 90''$), both the central (barred) and external (nonbarred) regions of the galaxy contribute to the integrals, while for large offsets ($y > 90''$), the integration axis does not cross the barred region and only the outer parts of the disk contribute to the pattern speed calculations. If the bar and spiral arms had significantly different pattern speeds, we would expect the T-W method to fail for small offsets. However, excluding the discrepant points 0″–200″ on the northeast side of the galaxy (which we attribute to a large H I cloud; see § 3.2), the pattern speed measurements yield a relatively constant value for all offsets and for most reasonable combinations of parameters. Considering the relatively small extent of the barred region and the importance of the flux in the outer parts of the disk, it might appear that the spiral arms dominate the contribution to the integrals in equation (1) even in the central regions. This is not so, however. For small offsets, both the inner barred region and the outer parts of the disk contribute significantly to the numerator. It is therefore very likely that a unique pattern speed is being measured. This view is further strengthened by the fact that the spiral arms in NGC 2915 appear to start from the end of the bar (although Sellwood & Sparke 1988 showed that this is not a strong argument).

We therefore adopt the view that the pattern speed we have measured in § 3.2 is the unique, common pattern speed of both the bar and the spiral arms, although we cannot entirely exclude the possibility that it is the pattern speed of the spiral arms alone.

5. ORIGIN OF THE PATTERN

Many theories exist to explain the formation of bar and spiral patterns in disk galaxies. We will now focus on the most popular ones. We note that the issue of the origin of the pattern in NGC 2915 is largely independent of the measured pattern speed. For example, is the pattern a phenomenon of the disk itself, or is it driven by external effects? We will show that the existence of a pattern in NGC 2915 is somewhat problematic.

5.1. *Gravitational Interactions*

Tidal triggering is a potentially important way to form bars, especially in dense environments. In the case of parabolic prograde planar encounters, Noguchi (1987) finds that self-consistent disks (with a static halo) develop strong spiral structures over their entire length, with a barlike pattern in the inner regions. Gerin, Combes, & Athanassoula (1990) showed that interaction with a companion accelerates bar formation. The sense of interaction (prograde or retrograde) affects the bar growth rate and shape, with lesser effects on the strength and pattern speed of the resulting bar. When a bar already exists, its strength and pattern speed can also be affected by an interaction.

It seems unlikely that such interaction scenarios can explain the structure seen in the H I disk of NGC 2915. No evidence of interaction is seen in the H I data of MCBF96 (although such an event could have occurred a long time ago). The only potential interaction partner cataloged within 5° of NGC 2915 is a low-luminosity, low surface brightness object, SGC 0938.1−7623, at a radius of 42′ (projected distance of 65 kpc at the distance of NGC 2915). This object does not have a cataloged optical or H I velocity, however, so although there are no indications that NGC 2915 is interacting, we cannot definitively exclude this possibility.

5.2. *Swing Amplification*

Swing amplification (Toomre 1981) can generate spiral arms in a disk as transient tidal features. Although Toomre (1981) considered a stellar disk, his treatment should apply equally to gaseous disks. Swing amplification is a local, cooperative effect: shear, epicyclic motions, and self-gravity all contribute to support the spiral pattern, originally excited by a small disturbance. In short, the epicyclic motions resonate with the shear flow as the spiral pattern

wraps, and the spiral arms are sustained. The self-gravity of the arms then leads to a gravitational instability (Goldreich & Lynden-Bell 1965). The effect can be quantified with Toomre's parameter X, given by

$$X = \lambda/\lambda_{\rm crit} , \tag{3}$$

where

$$\lambda_{\rm crit} = 4\pi^2 G\mu/\kappa^2 , \tag{4}$$

μ is the surface density, and κ is the epicyclic frequency. Swing amplification is efficient for $X \lesssim 3$; see, e.g., Fig. 7 of Toomre 1981). For an extended disk, we can write $\lambda = 2\pi r/m$, where m is the azimuthal wavenumber of the spiral pattern considered, and

$$X(r) = \frac{r\kappa(r)^2}{2\pi G m \mu(r)} \tag{5}$$

(see Athanassoula, Bosma, & Papaioannou 1987).

Figure 5 shows $X(r)$ for NGC 2915 for two- and four-armed spiral patterns. We use here only the surface density of the luminous matter (gaseous and stellar), assuming that the dark matter is not responsive to the density perturbation created by the spiral pattern (Toomre 1981 considered a fixed halo). In Figure 5*a*, only the H I distribution from MCBF96 is included (uncorrected for inclination; see Table 2). It is clear from the figure that $X(r)$ is nowhere near the value 3. In fact, even for $m = 4$, $X(r) \gtrsim 10$ for almost all radii. In Figure 5*b*, the stellar content is also included. To construct the stellar surface density profile, we used the B surface brightness profile of MMC94 for $r < 125''$ and an extrapolation of their exponential fit to the outer parts of the disk for larger radii: $B_c(0) = 21.79$ mag arcsec^{-2} (corrected for extinction but not inclination) and $\alpha_B^{-1} = 25''.6$, with $M/L_B = 1.2(M/L_B)_\odot$ (as in the adopted mass model of MCBF96). The resulting surface brightness profile is tabulated in Table 2. Even with the stellar component, $X(r) \gtrsim 10$ for most radii. Any correction for inclination would further decrease the importance of luminous matter. Small values of $X(r)$ are present only in the inner regions: $X(r) \leq 5$ only for $r < 75''$. We note, however, that those regions are within the rapidly rising portion of the rotation curve, where the bar resides and the shear is low, while swing amplification relies on shear to amplify the spiral pattern.

Toomre's (1981) work refers to a flat rotation curve, $V_c(r) = $ constant, which is not exactly the case here. The amplification criterion $X \lesssim 3$ increases for higher shear rates [e.g., $X \lesssim 6$ for a Keplerian rotation curve, $V_c(r) \propto r^{-1/2}$] and decreases for smaller shear [for example, $X \lesssim 1.5$ for $V_c(r) \propto r^{1/2}$; A. Toomre 1997, private communication]. The constraints on swing amplification are thus even stronger in the case of NGC 2915, especially in the inner parts.

Toomre's (1964) stability parameter Q also affects the efficiency of the swing amplifier mechanism. The stellar disk of NGC 2915 does not extend into the spiral pattern region, so we consider only the gaseous disk. Then,

$$Q(r) = \frac{v_s(r)\kappa(r)}{\pi G\mu(r)} , \tag{6}$$

where v_s is the sound speed of the gas, taken here to be the velocity dispersion. As Q increases, the maximum swing amplification factor decreases. For $V_c(r) = $ const, $Q \gtrsim 2$ curbs most of the amplification (see, again, Fig. 7 of Toomre 1981). The criterion becomes $Q \gtrsim 3$ for $V_c(r) \propto r^{-1/2}$ and $Q \gtrsim 1.5$ for $V_c(r) \propto r^{1/2}$ (A. Toomre 1997, private communication). Figure 6 shows $Q(r)$ for NGC 2915 using both a constant velocity dispersion (equal to the velocity dispersion in the outer parts of the H I disk) and the H I velocity dispersion profile of MCBF96, tabulated in Table 2. We see that $Q(r) \gtrsim 5$ everywhere, so the amplification factor would be small. In particular, Q is high in the inner regions. The sound speed would have to be less than 2–3 km s^{-1} to make $Q < 2$ over a significant range of radii. Even then, X would still be too high for the swing amplifier to work efficiently.

Given the behavior of $X(r)$ and $Q(r)$, and if the analogy between Toomre's (1981) stellar treatment and the gaseous

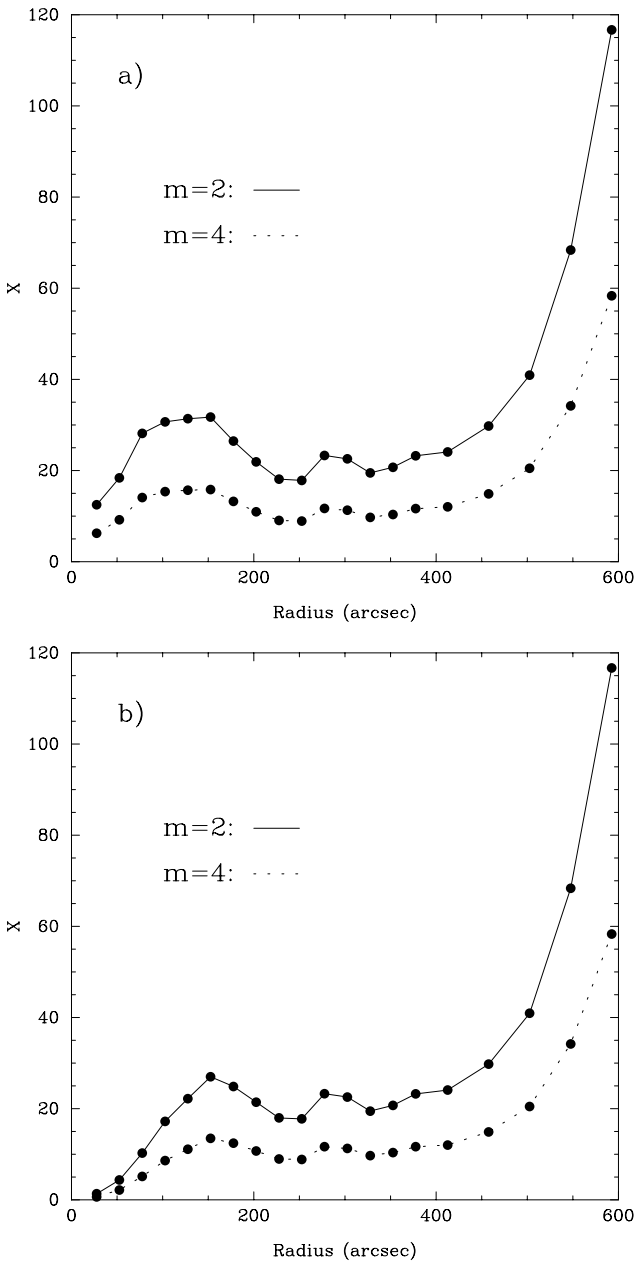

FIG. 5.—Calculated swing amplifier parameter $X(r)$ (eq. [5]) for two-armed ($m = 2$, *solid lines*) and four-armed ($m = 4$, *dotted lines*) spiral patterns in NGC 2915. In (*a*), only the H I distribution is taken into account. In (*b*), both the H I and the stellar component are considered. $X \lesssim 3$ is required for swing amplification.

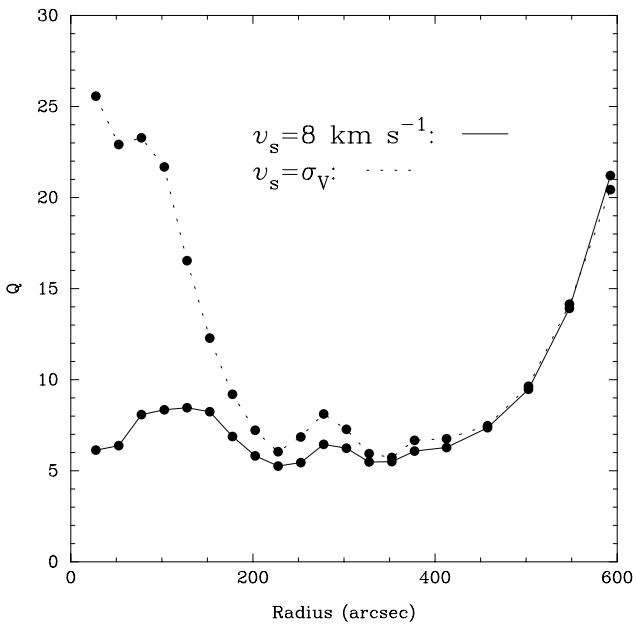

FIG. 6.—Calculated stability parameter $Q(r)$ (eq. [6]) in NGC 2915. *Solid line*, fixed sound speed $v_s(r) = 8$ km s^{-1}, equal to the velocity dispersion in the outer parts of the H I disk; *dotted line*, $v_s(r) = \sigma_v(r)$. $Q(r)$ scales directly with $v_s(r)$. $Q \gtrsim 2$ curbs swing amplification.

treatment adopted here is at least qualitatively valid,[3] it is clear that swing amplification cannot explain the spiral pattern seen in the disk of NGC 2915. We note that both X and Q scale inversely with the distance adopted, so a large error in the distance could weaken or invalidate our conclusion (if the real distance is larger). However, the error estimate of MMC94 does not allow this (they quote $D = 5.3 \pm 1.6$ Mpc). A distance of at least 10–15 Mpc would be required to make swing amplification efficient. Furthermore, given the very extended mass distribution of NGC 2915, it is unlikely that the observed spiral pattern results from an edge mode, as discussed by Toomre (1981).

At this point, we conclude that the bar and spiral patterns in NGC 2915 are unlikely to be caused by gravitational interaction or swing amplification. We must therefore search for an alternative formation mechanism.

5.3. *Resonance Ring Formation*

The arms of spiral galaxies frequently wrap to form ring-like structures. The theory of resonance ring formation (Schwarz 1981, 1984; Byrd et al. 1994) relates the shapes and positions of these rings to resonances in the disks. An examination of the total H I map of NGC 2915 suggests the presence of two such rings. For a given rotation curve, the bar pattern speed determines the existence and position of the resonances and, therefore, the kind and extent of the orbit families present in the disk (Sellwood & Wilkinson 1993). We can thus use resonance ring theory to check if our pattern speed measurement is consistent with the location of the pseudorings seen in NGC 2915 and determine whether the spiral arms are driven by the bar.

Using MCBF96's circular velocity curve, we can calculate the angular frequency of circular motion Ω and the associated Lindblad precession frequencies $\Omega + \kappa/2$, $\Omega - \kappa/2$, and $\Omega - \kappa/4$ (see Table 2). These are shown in Figure 7, along with the measured pattern speed and the position of the pseudorings seen in the disk of NGC 2915.

The innermost points in Figure 7 are affected by beam smoothing and by the bar but suggest the presence of an ILR ($\Omega_p = \Omega - \kappa/2$) at $r < 50''$. Nuclear rings are believed to be associated with ILRs, and they usually form easily recognizable annuli of H II regions in the inner parts of galaxies; the shallower the rotation curve in the inner parts, the larger the nuclear ring formed (Byrd et al. 1994). However, no such ring is visible in the photometry of MMC94 or in the Fabry-Perot Hα images of Marlowe et al.

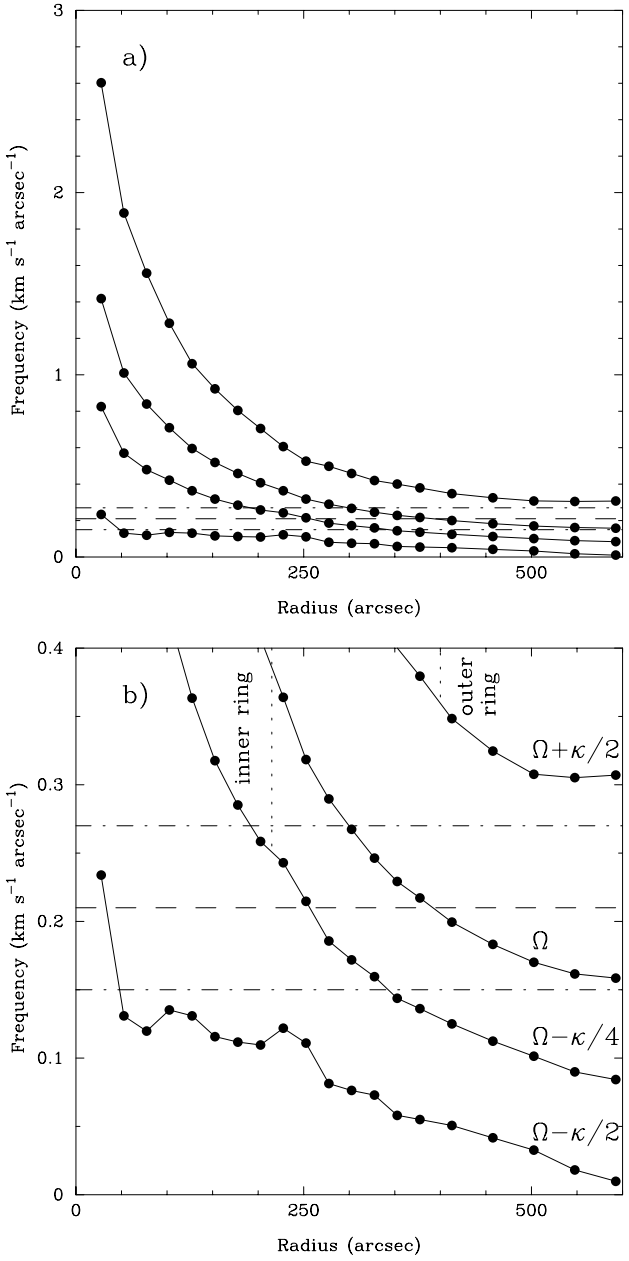

FIG. 7.—(*a*) Calculated Lindblad precession frequencies for NGC 2915 (*solid lines*). *Top to bottom*: $\Omega + \kappa/2$, Ω, $\Omega - \kappa/4$, and $\Omega - \kappa/2$; adopted pattern speed Ω_p (*dashed line*); range of values allowed by the uncertainty on Ω_p(*dot-dashed lines*). (*b*) An enlargement of (*a*) indicating the portion of various features in the disk of NGC 2915 (*vertical lines*).

[3] As mentioned by Toomre (1981), based on the work of Bardeen (1975) and Aoki, Noguchi, & Iye (1979), gaseous disks are probably more stable than stellar ones, which would strengthen our conclusions.

(1995). The resolution of MCBF96 H I data is too low to resolve a ring of radius smaller than about 1.5.

The inner spiral arms seen in the total H I intensity map of NGC 2915 (Fig. 3) appear to form a pseudoring just outside the end of the bar, at a deprojected radius of $215'' \pm 15''$. Inner rings are usually associated with the inner second harmonic resonance ($\Omega_p = \Omega - \kappa/4$), which in this case occurs between about 190″ and 340″. This is just consistent with the position of the inner pseudoring.

The outer spiral arms seen at the edge of the H I disk in Figure 3 form an outer pseudoring at $r = 400'' \pm 15''$. Outer rings are associated with the outer Lindblad resonance ($\Omega_p = \Omega + \kappa/2$), but the $\Omega + \kappa/2$ curve in Figure 7 does not intersect the range of measured values for Ω_p, which suggests that no outer Lindblad resonance is present in the disk of NGC 2915. Therefore, no outer ring would be expected.

Resonance ring theory has only limited success in explaining the position of the various pseudorings in NGC 2915 (nuclear, inner, and outer rings). It could be that the pattern of NGC 2915 is still evolving, and that the spiral arms are still in the process of forming the rings. This seems unlikely, however, since no nuclear ring is detected and the timescale for the formation of such rings is very short (10^7–10^8 yr; Combes 1993). Stellar mass loss or gas infall can also delay the formation of rings (Schwarz 1981), but these are improbable, as most of the H I disk is devoid of stars and NGC 2915 is isolated.

Petrou & Papayannopoulos (1986) proposed a mechanism to terminate bars well within their corotation radius. This mechanism requires the presence of a 1:1 resonance ($\Omega_p = \Omega - \kappa$) in the bar, however, so it is clear from Figure 7 that it is not relevant in the case of NGC 2915.

We conclude that the structures seen in the disk of NGC 2915 are probably not due to resonances and that the spiral pattern is not driven by the bar. In fact, from the positions of the inner and outer pseudorings, no single value of the pattern speed can be derived from resonance ring theory.

6. DARK MATTER AND THE STRUCTURE OF NGC 2915

The mass model of MCBF96 showed that NGC 2915 is dominated by dark matter even in the central (optical) regions of its disk. We now discuss the possible relations between the properties of this dominant dark matter distribution and the properties of the H I pattern.

6.1. *Rotationally Supported Disk Dark Matter*

Pfenniger, Combes, & Martinet (1994; see also Pfenniger & Combes 1994) proposed that the dark matter required dynamically in disk galaxies is in the form of rotationally supported cold molecular gas. This idea is attractive for NGC 2915 because it would also provide the extra disk mass needed to explain the formation of the bar and spiral arms through gravitational instabilities. Unfortunately, observing such cold gas directly is difficult (for H_2, see Combes & Pfenniger 1997; for CO, see Lequeux & Allen 1993 and Wilson & Mauersberger 1994).

Figure 8*a* shows how much additional mass is required in the disk for the swing amplification mechanism to be efficient ($X = 3$ everywhere in the disk; see § 5.2). Similarly, Figure 8*b* shows how much additional disk matter is required to lower Q to a value of 2 at all radii (the value required to make the disk gravitationally responsive). Again, those two values scale inversely (approximately) with distance. For comparison, we plot in Figure 8*c* the observed

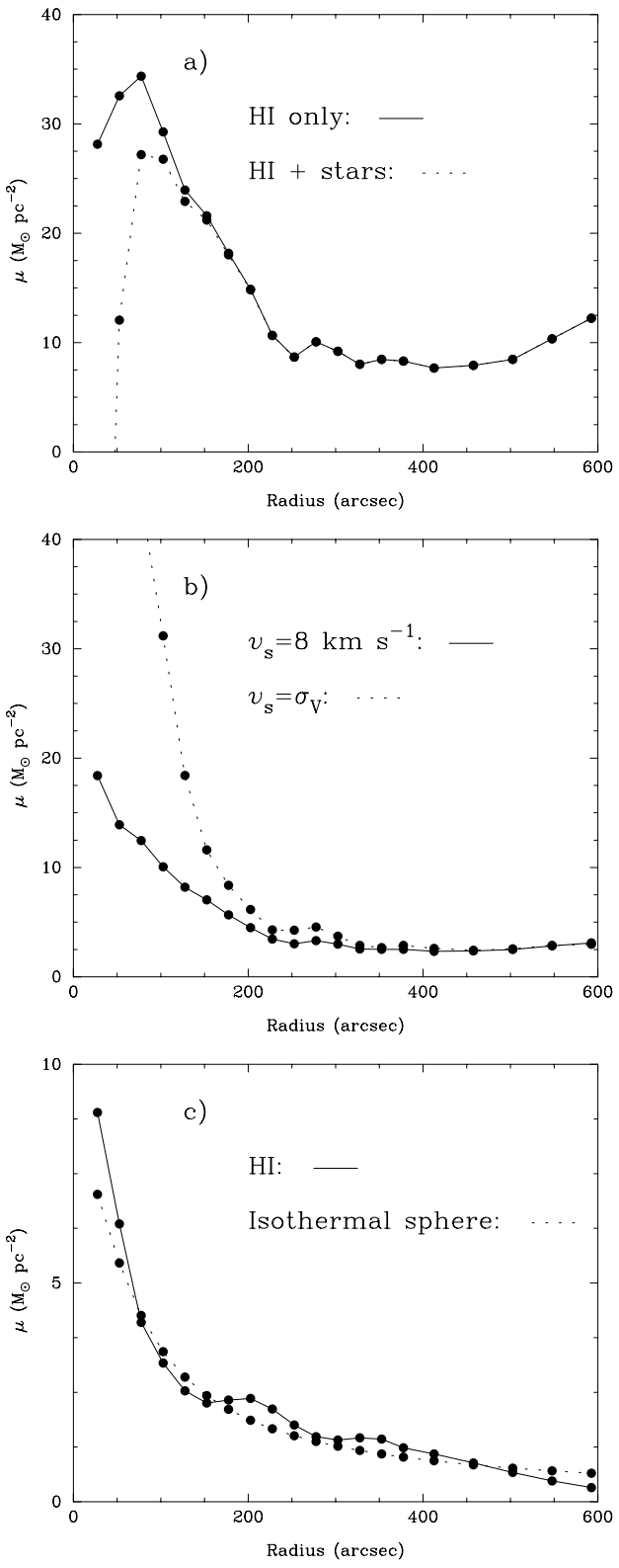

FIG. 8.—(*a*) Calculated disk dark matter surface density required to make the swing amplifier parameter $X(r) = 3$ (eq. [5]) for a two-armed ($m = 2$) spiral pattern in NGC 2915. *Solid line*, only the H I distribution is taken into account; *dotted line*, both the H I and the stellar component are considered. (*b*) Same as (*a*), but to make the stability parameter $Q(r) = 2$ (eq. [6]). *Solid line*, fixed sound speed $v_s(r) = 8$ km s^{-1}; *dotted line*, $v_s(r) = \sigma_v(r)$. $Q(r)$ scales directly with $v_s(r)$. (*c*) observed disk surface density (Table 2) of H I (*solid line*); μ_{DM}, the projected dark matter surface density of the dark isothermal sphere needed to model the rotation curve (model D of MCBF96, rescaled by 47.7) (*dotted line*).

H I surface density (Table 2) and the projected surface density of the dark isothermal sphere used by MCBF96 to model the circular velocity curve (their model D), rescaled by a large constant factor (47.7).

The similarity between the H I and the dark matter surface density profiles seen in Figure 8*c* has been noted in previous studies (Bosma 1978, 1981; Carignan & Beaulieu 1989; Broeils 1992) and has been interpreted as possible evidence that the H I and dark matter are somehow associated. Here we also see a qualitative similarity between the observed H I surface density profile and the surface density profile of the additional disk matter required to make $Q(r) = 2$ (Fig. 8*b*). It is tempting to regard this as further evidence that the dark matter is distributed in a disk and follows relatively closely the distribution of neutral hydrogen. However, the increase in disk surface density required to make the swing amplifier work efficiently ($X = 3$ over most of the disk; Fig. 8*a*) would lower Q even more and would make the disk unstable to axisymmetric modes. Figure 9 shows the ratio of the surface density obtained by imposing $X(r) = 3$ to Kennicutt's (1989) critical surface density for star formation in disks. This ratio is well above unity for the entire disk, so we would expect to see evidence of active star formation in the outer H I disk if the swing amplifier were working. However, Meurer et al. (1999) did not detect any Hα emission past $R_{\rm Ho}$. Their observations revealed only three faint H II regions near the Holmberg radius. These can be ionized by single late O or early A-type stars and are much fainter than those typically used to trace star formation in galaxies (as done by Kennicutt 1989). Therefore, at this point, it is unlikely that dark matter distributed in a disk can account for all the properties of NGC 2915 simultaneously.

It would be interesting to see this type of argument based on Toomre's (1964) Q-parameter and the presence of a spiral pattern be used more often in spiral galaxies, to test for the presence of substantial amount of unseen disk matter (see, e.g., Quillen & Pickering 1997; see also Quillen & Sarajedini 1998 for a similar application to intermediate-redshift galaxies).

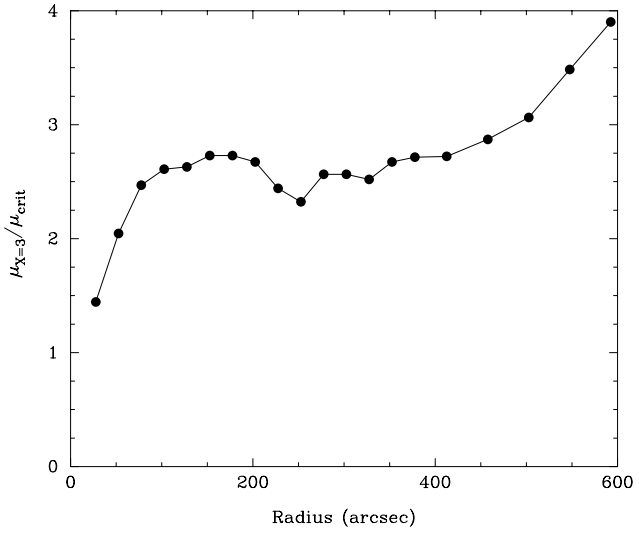

FIG. 9.—Calculated ratio of the total surface density required to make the swing amplifier parameter $X(r) = 3$ (eq. [5] with $m = 2$) to the critical surface density required for star formation in galactic disks (Kennicutt 1989).

6.2. *Slowly Rotating Triaxial Dark Halos*

Simulations of hierarchical structure formation in cold dark matter (CDM) universes produce the dark halos around galaxies that are triaxial in the mean, with some tendency to prolate shapes (Frenk et al. 1988; Warren et al. 1992; Dubinski & Carlberg 1991). The triaxiality and oblateness are slightly stronger in the outer parts but are almost independent of the halo mass and of the ratio V_r/σ_v (rotational velocity to velocity dispersion), indicating that the halos are supported by anisotropic velocity dispersions. The total angular momentum vectors are nevertheless preferentially aligned with the minor axes of the mass distributions at all radii. When dissipation is included, the halos become more oblate, while the flattening is unchanged (Dubinski 1994).

Observationally, the constraints on the shape of galactic halos remain weak. Polar ring galaxies (Sackett et al. 1994) and the flaring (Olling 1995) and warping (Sparke 1984a) of the outer H I disk of spirals are usually used to constrain the three-dimensional structure of halos. Such studies often indicate flattened and sometimes triaxial dark halos (see also Becquaert & Combes 1997; Olling 1996) but are as yet inconclusive.

We now consider the possibility that the dark halo of NGC 2915 is triaxial, with its figure rotating slowly about the rotation axis of the H I disk, and that the H I bar and spiral arms are due to the forcing of the H I disk by this massive, extended, and rotating triaxial halo. The halo would then act much like a very massive, slowly rotating bar. This would readily explain why there is a unique pattern speed for the bar and spiral arms and why the bar ends so far from corotation (see § 4). The situation that we are proposing is similar to that of rotating weak oval distortions in disks, which are able to maintain an open spiral pattern to large radii (see, e.g., Hunter et al. 1988). This is in contrast to a more conventional bar, where the quadrupole term decreases too rapidly outside corotation (where the bar ends) to maintain a spiral pattern. Hydrodynamic simulations of gaseous disks in large tumbling triaxial halos would be very useful to test our suggestion and to study the evolution of disks in such potentials.

The straight line of nodes of the warp in NGC 2915 (MCBF96) supports the suggestion of a triaxial halo. Displacements between the angular momentum vectors of the inner and outer regions of disks arise naturally in CDM models because of tidal torques. In an axisymmetric but flattened potential, the line of nodes would wrap quickly, but in a triaxial potential, the principal axes of the halo provide natural directions with which the warp can align (see Binney 1992 for a review of warps). Furthermore, an annulus of orbits circulating around the short axis of a triaxial halo becomes vertically unstable if the figure rotates, providing a natural way to excite a warp. However, this may happen too far out in the disk (outside corotation for prograde orbits) to be of interest here (see Binney 1978, 1981; see also Sparke 1984b).

While the studies mentioned above (Frenk et al. 1988; Warren et al. 1992; Dubinski & Carlberg 1991; Dubinski 1994) have shown that dark halos in CDM cosmological simulations can be strongly triaxial and have well-defined angular momentum properties (with flat rotation curves extending down to the core), only the instantaneous shapes and rotational motions within the figures (streaming) have

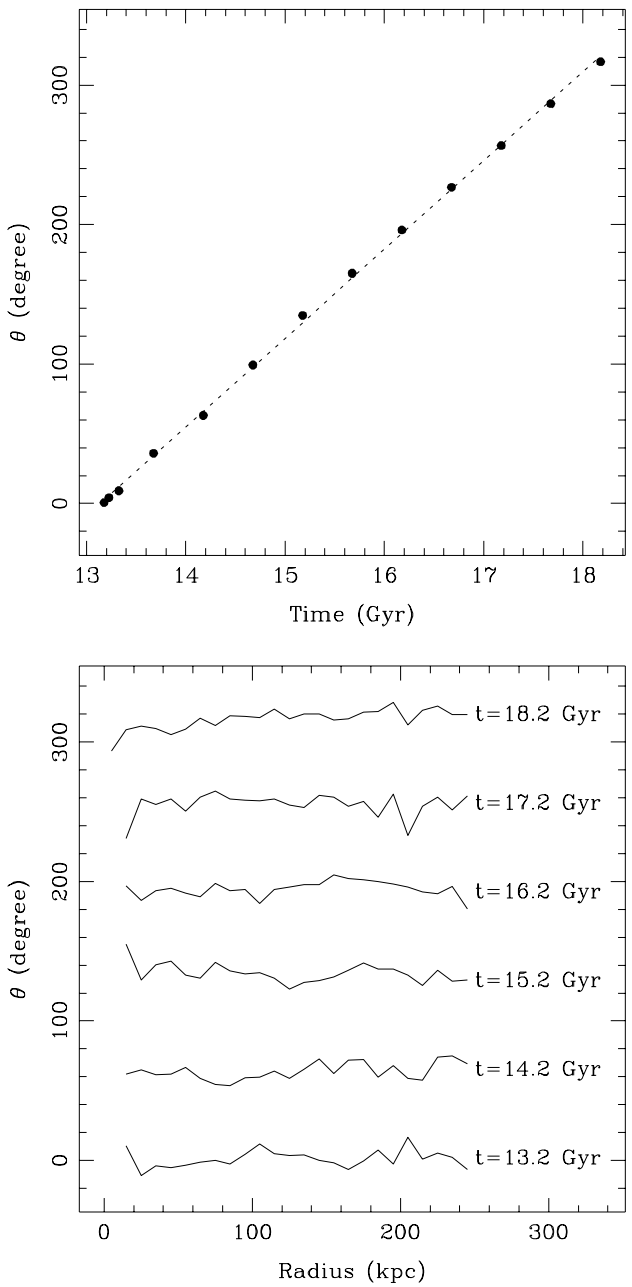

FIG. 10.—*Top*: Orientation of the major axis of a dark halo formed in a CDM simulation and evolved in isolation (see § 6.2) as a function of time. The angle θ is measured in a fixed plane perpendicular to the minor axis (the rotation axis). *Circles*, mean orientation of the halo as a function of time; *line*, linear fit to the data. *Bottom*: Orientation of the major axis of the halo as a function of radius (in isodensity-defined shells) for selected times. The halo rotates as a solid body.

been studied. As far as we are aware, no systematic study of the *figure* rotation of these triaxial halos has yet been carried out.

Pfitzner (2000) began a study of the figure rotation of halos in a set of large dissipationless CDM structure formation simulations. The halo shape distribution varies systematically with both radius and mass, but for our current purposes it suffices to say that many halos are significantly triaxial, as in other studies. Following the orientation of each halo over time, Pfitzner finds that a subset of triaxial halos exhibits steady figure rotation about their minor axis. The statistics of how many halos in the simulations have figure rotation is confused by numerical resolution issues, but the fraction is clearly significant. To verify that these results are not due to transient phenomena, one of the rotating halo candidates was extracted from the simulations at a time near the final epoch ($\approx$13 Gyr), and it was evolved in isolation. The halo displayed no systematic change of density or shape over a time of 5 Gyr. Figure 10 shows that the figure of this triaxial halo rotates as a solid body with constant pattern speed over the entire time span. Hence we conclude that at least some halos in these CDM simulations do exhibit genuine steady slow figure rotation over a Hubble time. However, because the halos formed are much more massive than that of NGC 2915, these simulations are not yet directly applicable to systems of that size. They do, however, suggest that an underlying triaxial dark halo with figure rotation could make an important contribution to the dynamics of the outer H I disk of some galaxies. If this is correct, it also offers another possibility to measure the shape of (triaxial) dark halos from detailed H I velocity fields, using methods similar to those of Franx, van Gorkom, & de Zeeuw (1994).

The slow pattern speeds found in the present study and in the above simulations are interesting in the context of the recent work by Miwa & Noguchi (1998). They made N-body simulations of barred galaxies in which the bars arose (1) spontaneously in marginally stable disks and (2) through the effect of a tidal interaction in more stable disks. The pattern speeds of the spontaneous bars are fast, with corotation near the ends of the bars, as generally expected in self-consistent systems. In the tidally induced bars, however, the pattern speeds are mostly much slower, and the bars appear to be limited by the ILR rather than by corotation. In particular, any relatively large tidal disturbance leads to a slow pattern speed, independent of the original properties of the disk. These results may be relevant to the pattern speeds of the triaxial dark halos formed in CDM simulations, in which the triaxiality results at least partially from tidal effects during the aggregation process.

Although more speculative, it may also be that triaxial halos are an essential ingredient for the formation of starbursts. We may then be witnessing in NGC 2915 the buildup of a bulge, as gas driven to the center by the triaxial halo potential gradually is transformed into stars by the central starburst. The diffuse red stellar population detected by MMC94 argues however for an even earlier burst of star formation. Nevertheless, if all the H I were turned into stars, NGC 2915 would appear very much like a normal spiral galaxy, with an "old" bulge and a young disk that obeys the Tully-Fisher relation [Tully & Fisher 1977; assuming $M/L_B = 1\ (M/L_B)_\odot$ for the gas]. In this picture, the gaseous disk of NGC 2915 would be almost pristine.

7. CONCLUSION

We have used the method of Tremaine & Weinberg (1984) to measure the pattern speed of the disk in the galaxy NGC 2915, using neutral hydrogen as the tracer and radio synthesis data. NGC 2915 is a BCD galaxy with a very extended H I disk showing an open barred spiral morphology. It is also strongly dominated by dark matter. Our measurements yield a pattern speed of 8.0 ± 2.4 km s^{-1} kpc^{-1} for $D = 5.3$ Mpc. This pattern speed is inconsistent with the general property of self-consistent barred disks that corotation occurs just outside the end of the bar. However,

it agrees well with more recent models considering dark halos with high central densities. Our adopted bar length puts corotation at more than 1.7 bar radii. We considered the possibility that the bar and spiral arms have different pattern speeds but demonstrated that this is unlikely.

Independent of its pattern speed, the existence of the bar and spiral pattern observed in NGC 2915 is also hard to understand. NGC 2915 is isolated, so gravitational interactions are unlikely to explain the strong pattern observed in the H I disk. Because the surface density in the disk is so low, Toomre's (1981) swing amplification mechanism is also unable to explain the origin of the structures. Furthermore, resonance ring theory fails to predict successfully the position of the pseudorings seen in the disk of NGC 2915, indicating that the spiral arms are not driven by the bar itself.

This led us to consider two scenarios to explain both the structure and dynamics of the H I disk in NGC 2915. First, we considered dark matter in nearly circular motion, distributed in a disk, and following closely the distribution of H I, as suggested by the similarity of the dark matter and H I surface density profiles. This does not appear to work: if the dark matter disk is dense enough for the swing amplifier to work efficiently, then the disk becomes unstable to axisymmetric disturbances and we would expect to see evidence of active star formation, which is not observed. Second, we considered the effects of dark matter distributed in a massive pressure-supported halo with extended triaxiality, like the halos seen in CDM cosmological simulations. In addition, we required the halo to have a slow figure rotation. Such figure rotation is seen in the preliminary analysis of a set of CDM simulations. These show triaxial halos with figure rotation constant over many gigayears. This kind of model has the potential to explain the structures seen in the disk of NGC 2915, through the torques exerted by the slowly rotating triaxial figure on the disk.

The structure in the H I disk of NGC 2915 is visible because the radio synthesis observations were made at a relatively high spatial resolution (beam FWHM of about 650 pc for the uniformly weighted data and about 1150 pc for the naturally weighted data). As far as we are aware, NGC 2915 is the only galaxy showing such structure in an extended H I disk. If our suggestions are correct, it would be very desirable to obtain H I observations of similar spatial resolution for other nearby galaxies with extended H I disks, as they may provide similar insight into the dynamics of their dark halos. Our argument on figure rotation also relies heavily on the theory of forcing of structures by oval distortions, in a situation that is not precisely analogous to that in NGC 2915. Hydrodynamic simulations of gas disks in the potentials of triaxial halos with figure rotation would thus be very welcome.

We thank A. J. Kalnajs for comments on the manuscript and D. Pfenniger, J. A. Sellwood, and V. P. Debattista for useful discussions. M. Bureau acknowledges the support of an Australian DEETYA Overseas Postgraduate Research Scholarship and a Canadian NSERC Postgraduate Scholarship during the conduct of this research. The Digitized Sky Surveys were produced at the Space Telescope Science Institute under US government grant NAGW-2166. The images of these surveys are based on photographic data obtained using the Oschin Schmidt Telescope on Palomar Mountain and the UK Schmidt Telescope. The plates were processed into the present compressed digital form with the permission of these institutions.

REFERENCES

Aoki, S., Noguchi, M., & Iye, M. 1979, PASJ, 31, 737
Athanassoula, E. 1992a, MNRAS, 259, 328
———. 1992b, MNRAS, 259, 345
Athanassoula, E., Bosma, A., & Papaioannou, S. 1987, A&A, 179, 23
Athanassoula, E., & Sellwood, J. A. 1986, MNRAS, 221, 213
Bardeen, J. M. 1975, in Dynamics of Stellar Systems, ed. A. Hayli (Dordrecht: Reidel), 297
Becquaert, J.-F., & Combes, F. 1997, A&A, 325, 41
Begeman, K. G. 1989, A&A, 223, 47
Binney, J. J. 1978, MNRAS, 183, 779
———. 1981, MNRAS, 196, 455
———. 1992, ARA&A, 30, 51
Bosma, A. 1978, Ph.D. thesis, Univ. Groningen
———. 1981, AJ, 86, 1791
Broeils, A. H. 1992, A&A, 256, 19
Byrd, G. G., Ousley, D., & Dalla Piazza, C. 1998, MNRAS, 298, 78
Byrd, G., Rautiainen, P., Salo, H., Buta, R., & Crocker, D. A. 1994, AJ, 108, 476
Canzian, B. 1993, ApJ, 414, 487
Carignan, C., & Beaulieu, S. 1989, ApJ, 347, 760
Carignan, C., & Freeman, K. C. 1985, ApJ, 294, 494
Carr, B. 1994, ARA&A, 32, 531
Combes, F. 1993, in *N*-Body Problems and Gravitational Dynamics, ed. F. Combes & E. Athanassoula (Paris: Obs. Paris), 137
Combes, F., & Pfenniger, D. 1997, A&A, 327, 453
Combes, F., & Sanders, R. H. 1981, A&A, 96, 164
Contopoulos, G. 1980, A&A, 81, 198
Contopoulos, G., & Grosbøl, P. 1989, A&A Rev., 1, 261
Debattista, V. P., & Sellwood, J. A. 1998, ApJ, 493, L5
Dubinski, J. 1994, ApJ, 431, 617
Dubinski, J., & Carlberg, R. G. 1991, ApJ, 378, 496
Elmegreen, B. 1996, in ASP Conf. Ser. 91, Barred Galaxies, ed. R. Buta, D. A. Crocker, & B. G. Elmegreen (San Francisco: ASP), 197
Franx, M., van Gorkom, J. H., & de Zeeuw, T. 1994, ApJ, 436, 642
Frenk, C. S., White, S. D. M., Davis, M., & Efstathiou, G. 1988, ApJ, 327, 507
Gerin, M., Combes, F., & Athanassoula, E. 1990, A&A, 230, 37
Gerssen, J., Kuijken, K., & Merrifield, M. R. 1999, MNRAS, 306, 926
Goldreich, P., & Lynden-Bell, D. 1965, MNRAS, 130, 125
Hunter, J. H., Ball, R., Huntley, J. M., England, M. N., & Gottesman, S. T. 1988, ApJ, 324, 721
Kalnajs, A. J. 1971, ApJ, 166, 275
———. 1977, ApJ, 212, 637
Kennicutt, R. C., Jr. 1989, ApJ, 344, 685
Kent, S. M. 1987, AJ, 93, 1062
———. 1990, AJ, 100, 377
Kormendy, J. 1984, ApJ, 286, 132
Kuijken, K., & Merrifield, M. R. 1996, in ASP Conf. Ser. 91, Barred Galaxies, ed. R. Buta, D. A. Crocker, & B. G. Elmegreen (San Francisco: ASP), 215
Lequeux, J., & Allen, R. J. 1993, A&A, 280, L23
Lindblad, P. A. B., & Kristen, H. 1996, A&A, 313, 733
Lindblad, P. A. B., Lindblad, P. O., & Athanassoula, E. 1996, A&A, 313, 65
Marlowe, A. T., Heckman, T. M., Wyse, R. F. G., & Schommer, R. 1995, ApJ, 438, 563
Merrifield, M. R., & Kuijken, K. 1995, MNRAS, 274, 933
Meurer, G. R., Carignan, C., Beaulieu, S. F., & Freeman, K. C. 1996, AJ, 111, 1551 (MCBF96)
Meurer, G. R., Freeman, K. C., Bland-Hawthorn, J., Knezek, P. M., & Allen, R. J. 1999, BAAS, 31, 828
Meurer, G. R., Mackie, G., & Carignan, C. 1994, AJ, 107, 2021 (MMC94)
Miwa, T., & Noguchi, M. 1998, ApJ, 499, 149
Noguchi, M. 1987, MNRAS, 228, 635
Olling, R. P. 1995, AJ, 110, 591
———. 1996, AJ, 112, 481
Petrou, M., & Papayannopoulos, T. 1986, MNRAS, 219, 157
Pfenniger, D., & Combes, F. 1994, A&A, 285, 94
Pfenniger, D., Combes, F., & Martinet, L. 1994, A&A, 285, 79
Pfitzner, D. W. 2000, in preparation
Quillen, A. C., & Pickering, T. E. 1997, AJ, 113, 2075
Quillen, A. C., & Sarajedini, V. L. 1998, AJ, 115, 1412
Raha, N., Sellwood, J. A., James, R. A., & Kahn, F. D. 1991, Nature, 352, 411
Ryder, S. D., Buta, R. J., Toledo, H., Shukla, H., Staveley-Smith, L., & Walsh, W. 1996, ApJ, 460, 665
Sackett, P. D., Rix, H.-W., Jarvis, B. J., & Freeman, K. C. 1994, ApJ, 436, 629
Sancisi, R., Allen, R. J., & Sullivan, W. T. 1979, A&A, 78, 217

Schmidt, K.-H., & Boller, T. 1992, Astron. Nachr., 313, 189
Schwarz, M. P. 1981, ApJ, 247, 77
———. 1984, MNRAS, 209, 93
Seiger, M. S., & James, P. A. 1998, MNRAS, 299, 672
Sellwood, J. A. 1980, A&A, 89, 296
———. 1981, A&A, 99, 362
Sellwood, J. A., & Sparke, L. S. 1988, MNRAS, 231, 25P
Sellwood, J. A., & Wilkinson, A. 1993, Rep. Prog. Phys., 56, 173
Sparke, L. S. 1984a, ApJ, 280, 117
———. 1984b, MNRAS, 211, 911
Sparke, L. S., & Sellwood, J. A. 1987, MNRAS, 225, 653
Sygnet, J. F., Tagger, M., Athanassoula, E., & Pellat, R. 1988, MNRAS, 232, 733
Tagger, M., Sygnet, J. F., Athanassoula, E., & Pellat, R. 1987, ApJ, 318, L43
Teuben, P. J., & Sanders, R. H. 1985, MNRAS, 212, 257
Toomre, A. 1964, ApJ, 139, 1217
———. 1981, in Structure and Evolution of Normal Galaxies, ed. S. M. Fall & D. Lynden-Bell (Cambridge: Cambridge Univ. Press), 111
Tremaine, S., & Weinberg, M. D. 1984, ApJ, 282, L5
Trimble, V. 1987, ARA&A, 25, 425
Tully, R. B., & Fisher, J. R. 1977, A&A, 54, 661
Warren, M. S., Quinn, P. J., Salmon, J. K., & Zurek, W. H. 1992, ApJ, 399, 405
Weinberg, M. D. 1985, MNRAS, 213, 451
Wilson, T. L., & Mauersberger, R. 1994, A&A, 282, L41